Dimensional Analysis of the Pounding Response of an Oscillator Considering Contact Duration

Changhai Zhai[1]; Shan Jiang[2]; and Zhiqiang Chen[3]

Abstract: The dynamic response of an elastic pounding oscillator subjected to harmonic excitation is investigated with dimensional analysis. To model the pounding process, a linear viscoelastic model is used to simulate the contact force. Through dimensional analysis, the peak structural response parameters of the pounding oscillator, including structural displacement, velocity, and penetration displacement, are characterized by a set of dimensionless terms (denoted by the Buckingham notation Π). The reduced Π-set explicitly describes the interaction between the oscillator and the rigid barrier. Analytical solutions to dimensionless contact time, displacement, and velocity response are derived in this study and are further verified against the numerical simulation. The effect of pounding on the oscillator's response is illustrated using three well-divided spectral regions (i.e., amplified, deamplified, and unaffected regions), which are defined based on the dimensionless system frequency parameter Π_ω. Parametric studies show that the penetration displacement for different levels of contact stiffness is insensitive to the dimensionless gap size Π_d but is affected significantly by changes in the coefficient of restitution Π_r. **DOI: 10.1061/(ASCE)EM.1943-7889.0000858.**

Author keywords: Pounding; Dimensional analysis; Earthquake engineering; Elastic oscillator.

Introduction

Numerous investigators have reported that pounding between adjacent structures is one of the main reasons for structural damage during earthquakes (Anagnostopoulos 1995, 1996; Jeng and Tzeng 2000). For example, over 15% of the 330 collapsed or severely damaged structures in the 1985 Mexico City earthquake were caused by pounding (Rosenblueth and Meli 1986). During the 1989 Loma Prieta earthquake, over 200 pounding instances were observed involving more than 500 buildings (Kasai and Maison 1997). During the 1995 Kobe earthquake, many buildings were severely damaged because of the pounding interaction between adjacent structures (Comartin et al. 1995). And during the 2008 Wenchuan earthquake, pounding-related damage also was observed between many adjacent structures (Li et al. 2008).

In general, two different approaches are used to simulate collision between adjacent buildings. The first is based on the impact laws of mechanics, with a coefficient of restitution (Papadrakakis et al. 1991; Athanassiadou et al. 1994; Malhotra 1998; DesRoches and Muthukumar 2002). Davis (1992) derived the closed-form solution to impact velocity for a single oscillator interacting with a rigid barrier. The work of Davis was extended by Chau and Wei (2001), who investigated pounding between two single-degree-of-freedom (SDOF) oscillators. The analytical solutions obtained in these two efforts were both based on the stereomechanical approach. However, if the duration of impact is long enough, this approach is no longer valid because it does not consider transient stresses and deformations in the impacting bodies (Jankowski 2005; Muthukumar and DesRoches 2006).

The second approach directly models the pounding force by a contact-element method. This approach is a force-based approach that considers the deformation of the colliding bodies and can provide a better approximation of the real contact physics (Anagnostopoulos 1995). The most frequently used impact element is a linear viscoelastic model because of its simplicity and the clearly defined mathematical relationship between the element's damping ratio and the coefficient of restitution (Anagnostopoulos and Spiliopoulos 1992; Jankowski et al. 1998).

Pounding is a highly nonlinear process involving numerous material and geometric variables. As such, one of the major challenges in studying the pounding response is to grapple with the large and wide variety of parameters that govern the response of pounding structures, which has resulted in some conflicting conclusions in the literature. One of the promising approaches to dealing with this parametric complexity in the field of earthquake engineering research is dimensional analysis, which offers a condensed presentation of the seismic response and brings forward the fundamental physical similarities that describe the structural behavior. Using dimensional analysis, Makris and Black (2004a, b) and Makris and Psychogios (2006) revisited the inelastic response of elastoplastic and bilinear systems under pulse-type excitations; Zhang and Tang (2009) evaluated the inertial soil-structure interaction effects on linear and bilinear structures subjected to near-fault ground motions. In addition, Dimitrakopoulos et al. (2009, 2010, 2011) introduced the dimensional analysis approach into the study of structural pounding for elastic and inelastic oscillators subjected to distinct pulses based on the impact laws of mechanics with a coefficient of restitution. Different from Dimitrakopoulos's work, the contact-element method is used in this paper, which considers the deformation of colliding bodies and can trace the structural response during the contact.

In this paper, the pounding response of a single oscillator against a rigid barrier subjected to harmonic excitations is investigated with dimensional analysis. To trace the structural response during contact,

[1]Professor, School of Civil Engineering, Harbin Institute of Technology, Harbin 150090, China (corresponding author). E-mail: zch-hit@hit.edu.cn

[2]Ph.D. Candidate, School of Civil Engineering, Harbin Institute of Technology, Harbin 150090, China. E-mail: shjiang.hit@gmail.com

[3]Assistant Professor, School of Civil and Mechanical Engineering, Univ. of Missouri, Kansas City, MO 64110-2499. E-mail: chenzhiq@umkc.edu

Note. This manuscript was submitted on August 27, 2013; approved on August 4, 2014; published online on September 8, 2014. Discussion period open until February 8, 2015; separate discussions must be submitted for individual papers. This paper is part of the ***Journal of Engineering Mechanics***, © ASCE, ISSN 0733-9399/04014138(10)/$25.00.

the linear viscoelastic model is adopted. Analytical solutions to dimensionless contact time, displacement, and velocity, expressed by the dimensionless Π-parameters, are derived in this study, and numerical simulations are carried out to examine the applicability of the analytical solution. Parametric studies are conducted to assess the effects of contact stiffness, gap distance, coefficient of restitution, and frequency ratio of the oscillator to excitation on the structural pounding responses.

Mathematical Models

Modeling of Pounding Force

The model of dynamic pounding between a single oscillator and a rigid barrier at a distance d is shown in Fig. 1. The oscillator is characterized by mass m, lateral stiffness k, and damping coefficient c. The relative displacement of the oscillator to the ground is X, with the direction toward the barrier defined as positive. The ground motion is simply treated, and sinusoidal excitation is used to represent seismic ground motions. The pounding force F during impact is expressed based on the linear viscoelastic model (Anagnostopoulos 1988)

$$F = \begin{cases} \beta \cdot \Gamma + \overline{c} \cdot \dot{\Gamma} & \Gamma \geq 0 \\ 0 & \Gamma < 0 \end{cases} \tag{1}$$

where Γ = penetration deformation of colliding members ($=X-d$); $\dot{\Gamma}$ = relative velocity (the superimposed dot denotes the derivative with respect to time t); β = impact element's local stiffness at the contact point, which is a function of the elastic properties and geometry of the contact bodies (Goldsmith 1960); and $\overline{c}$ = impact element's damping coefficient, which can be obtained from the following equation (Anagnostopoulos 2004):

$$\overline{c} = 2\overline{\zeta}\sqrt{\beta \frac{m \cdot m_2}{m + m_2}} \tag{2}$$

Because the mass of barrier m_2 is assumed to be much greater than that of the oscillator, i.e., $m/m_2 \to 0$, damping $\overline{c}$ can be simplified as

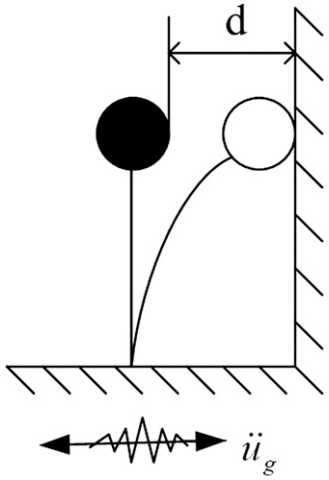

Fig. 1. Model configuration of single-impact oscillator subjected to excitation

$$\overline{c} = 2\overline{\zeta}\sqrt{\beta \cdot m} \tag{3}$$

where $\overline{\zeta}$ = damping ratio correlated with the coefficient of restitution r, which is defined as (Anagnostopoulos 2004)

$$\overline{\zeta} = -\frac{\ln r}{\sqrt{\pi^2 + (\ln r)^2}} \tag{4}$$

The coefficient of restitution expresses the inelasticity of impact. A value of $r = 1$ corresponds to the case of a fully elastic collision, whereas a value of $r = 0$ corresponds to a fully plastic collision.

The linear viscoelastic model has a shortcoming that results in negative impact force toward the end of contact. However, this model has been used widely for the simulation of structural pounding because of its simplicity and the clearly defined mathematical relationship between the element's damping ratio and the coefficient of restitution. According to Jankowski (2005), the linear and nonlinear viscoelastic models have a similar precision in simulating the pounding-force time histories during impact. Because the simplicity of the linear viscoelastic model is beneficial and convenient for application of the dimension analysis method, the authors use the linear viscoelastic model in this study.

Equation of Motion

The equation of motion of a single pounding oscillator of mass m can be written as

$$m\ddot{X}(t) + c\dot{X}(t) + kX(t) + F(t) = -m\ddot{u}_g(t) \tag{5}$$

or, equivalently, as

$$\ddot{X}(t) + 2\zeta\omega\dot{X}(t) + \omega^2 X(t) + \frac{F(t)}{m} = -\ddot{u}_g(t) \tag{6}$$

where X = relative displacement of the oscillator; t = time; F = pounding force; and $\ddot{u}_g$ = seismic ground acceleration, which assumes a harmonic form

$$\ddot{u}_g(t) = a_p \cdot \sin(\omega_p \cdot t) \tag{7}$$

where a_p = acceleration amplitude; and ω_p = circular frequency. Indeed, the most realistic and efficient way to analyze the earthquake-induced pounding is to use real recorded ground motions, and the harmonic excitation is not a perfect approximation of real ground motions because of the complexity of earthquake ground motions. However, for the convenience of implementing dimensional analysis and deriving analytical solutions, harmonic excitation is adopted.

Eq. (6) can be rewritten in dimensionless form as

$$\ddot{x} + 2\zeta\frac{\omega}{\omega_p}\dot{x} + \frac{\omega^2}{\omega_p^2}x + \frac{F}{ma_p} = -\sin\tau \tag{8}$$

where the superimposed dot denotes the derivative with respect to normalized time τ. In Eq. (8), the normalized time variable τ and other definitions include

$$t = \frac{\tau}{\omega_p}, \quad X = l_e \cdot x = \frac{x \cdot a_p}{\omega_p^2}, \quad \dot{X} = \frac{\dot{x} \cdot a_p}{\omega_p}, \quad \zeta = \frac{c}{2m\omega}, \quad \omega^2 = \frac{k}{m} \tag{9}$$

where ω = natural frequency of the oscillator; and $l_e = a_p/\omega_p^2$ is a characteristic length scale of the ground excitation (Makris and Black 2004b).

Using the definitions in Eq. (9), the normalized pounding force F/ma_p is obtained

$$\frac{F}{ma_p}=\begin{cases}\dfrac{\overline{\omega}^2}{\omega_p^2}\cdot\left(x-\dfrac{d}{l_e}\right)+2\overline{\zeta}\dfrac{\overline{\omega}}{\omega_p}\cdot\dot{x} & x-\dfrac{d}{l_e}\geq 0\\ 0 & x-\dfrac{d}{l_e}<0\end{cases} \tag{10}$$

where $\overline{\omega}$ = circular frequency of the contact element, defined by

$$\overline{\omega}=\sqrt{\beta/m} \tag{11}$$

Based on Eqs. (8) and (10), when $x-d/l_e\geq 0$, a collision occurs; during this phase, the motion equation of the pounding oscillator is

$$\ddot{x}+2\left(\zeta\frac{\omega}{\omega_p}+\overline{\zeta}\frac{\overline{\omega}}{\omega_p}\right)\dot{x}+\left(\frac{\omega^2}{\omega_p^2}+\frac{\overline{\omega}^2}{\omega_p^2}\right)x=-\sin\tau+\frac{\overline{\omega}^2}{\omega_p^2}\cdot\frac{d}{l_e} \tag{12}$$

When $x-d/l_e<0$, no pounding occurs; the corresponding equation of the oscillator therefore is

$$\ddot{x}+2\zeta\frac{\omega}{\omega_p}\dot{x}+\frac{\omega^2}{\omega_p^2}x=-\sin\tau \tag{13}$$

Dimensional Analysis

Based on the preceding governing equations and definitions, the parameters governing the responses of a single pounding oscillator (i.e., the maximum response displacement $X_{\max}$, the maximum velocity $\dot{X}_{\max}$, and the maximum penetration displacement X_{con}) include the circular frequency of the oscillator ω, the damping ratio of the oscillator ζ, the pulse amplitude a_p, the circular frequency ω_p, the coefficient of restitution r, the gap size d, and the circular frequency of the contact element $\overline{\omega}$. Thus

$$X_{\max}\quad\text{or}\quad\dot{X}_{\max}\quad\text{or}\quad X_{\text{con}}=f\left(\zeta,r,\omega,\overline{\omega},d,\omega_p,a_p\right) \tag{14}$$

The eight variables in Eq. (14) involve only two reference dimensions, the length $[L]$ and the time $[T]$. According to Buckingham's Π theorem, the number of independent dimensionless Π-products can be reduced as $(8\text{ variables})-(2\text{ reference dimensions})=6\,\Pi$-parameters.

Herein, the dimensionally independent parameters a_p and ω_p are selected as repeating variables. Oscillator displacement is normalized by the energetic length scale of the excitation $l_e=a_p/\omega_p^2$, and velocity is normalized by a_p/ω_p. Accordingly, Eq. (14) reduces to

$$\frac{X_{\max}\omega_p^2}{a_p}\quad\text{or}\quad\frac{\dot{X}_{\max}\omega_p}{a_p}\quad\text{or}\quad\frac{X_{\text{con}}\omega_p^2}{a_p}=\phi\left(\zeta,r,\frac{\omega}{\omega_p},\frac{\overline{\omega}}{\omega_p},\frac{d\omega_p^2}{a_p}\right) \tag{15}$$

or

$$\Pi_u\quad\text{or}\quad\Pi_v\quad\text{or}\quad\Pi_{\text{ucon}}=\phi\left(\Pi_\zeta,\Pi_r,\Pi_\omega,\Pi_{\omega1},\Pi_d\right) \tag{16}$$

with

$$\Pi_u=\frac{X_{\max}\omega_p^2}{a_p},\quad\Pi_v=\frac{\dot{X}_{\max}\omega_p}{a_p},\quad\Pi_{\text{ucon}}=\frac{X_{\text{con}}\omega_p^2}{a_p},$$
$$\Pi_\zeta=\zeta,\quad\Pi_r=r,\quad\Pi_\omega=\frac{\omega}{\omega_p},\quad\Pi_{\omega1}=\frac{\overline{\omega}}{\omega_p},\quad\Pi_d=\frac{d\omega_p^2}{a_p} \tag{17}$$

The new terms proposed in this study to describe the pounding response are $\Pi_{\omega1}$ and Π_{ucon}. $\Pi_{\omega1}$ suggests that the circular frequency of the contact element can be scaled to the excitation. Some researchers (Maison and Kasai 1992; Jankowski et al. 1998; Muthukumar and DesRoches 2006) have employed the stiffness of the impact element as an axial stiffness of the superstructure segment. In this study, the product term $\Pi_{\omega1}$ can be used to choose the appropriate value of the impact stiffness, and Π_{ucon} means that the maximum penetration is scaled to the energetic length scale of the excitation a_p/ω_p^2.

Π_ζ is the damping ratio of the oscillator. Π_r is the coefficient of restitution, which is a dimensionless parameter describing the inelasticity of the impact. According to Eq. (4), the damping ratio of the contact element $\overline{\zeta}$ varies with Π_r. Π_ω is the natural frequency of the examined oscillator normalized to the frequency of the excitation. The product term Π_d proposed by Dimitrakopoulos et al. (2009, 2010) indicates the gap size that is normalized to the energetic length scale of the excitation a_p/ω_p^2.

Analytical Solution of Impact

Duration of Contact

The duration of contact is defined as the process from the moment the oscillator comes into contact with the barrier to the moment that the oscillator detaches from the barrier. The contact process with initial displacement $\Gamma(0)=0$ and velocity $\dot{\Gamma}(0)=V_0$ is shown in Fig. 2. The collision of the oscillator with the barrier is simulated with the spring-dashpot element, which is activated when the oscillator comes into contact with the barrier. The motion equation of the oscillator during the collision, when the impact element has been activated, is written as

$$m\ddot{\Gamma}(\bar{t})+c\dot{\Gamma}(\bar{t})+k\Gamma(\bar{t})+F(\bar{t})=0 \tag{18}$$

where the contact force F is defined in Eq. (1); and $\bar{t}$ = time for the penetration process, which is activated at the onset of contact. When $\bar{t}=0$, the oscillator begins to make contact with the barrier. When $\bar{t}=\Delta t$, the oscillator detaches from the barrier. Δt is the time span of contact. Eq. (18) can be rewritten in dimensionless form as

$$\ddot{\delta}(\overline{\tau})+2\left(\zeta\Pi_\omega+\overline{\zeta}\Pi_{\omega1}\right)\dot{\delta}(\overline{\tau})+\left(\Pi_\omega^2+\Pi_{\omega1}^2\right)\delta(\overline{\tau})=0 \tag{19}$$

where $\delta=\Gamma/l_e$ = normalized penetration displacement. The superimposed dot denotes the derivative with respect to normalized time $\overline{\tau}=\omega_p\cdot\bar{t}$.

The corresponding solutions to Eq. (19) can be obtained as follows:

$$\delta(\overline{\tau})=\left(c_1\cos\frac{\sqrt{-\Delta}}{2}\overline{\tau}+c_2\sin\frac{\sqrt{-\Delta}}{2}\overline{\tau}\right)e^{-\left(\zeta\Pi_\omega+\overline{\zeta}\Pi_{\omega1}\right)\overline{\tau}} \tag{20}$$

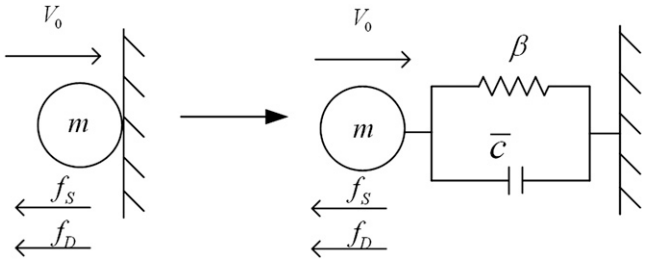

Fig. 2. Model of single-impact oscillator during contact process subjected to excitation

$$\dot{\delta}(\overline{\tau}) = -\left(\zeta\Pi_\omega + \overline{\zeta}\Pi_{\omega 1}\right)\left(c_1 \cos\frac{\sqrt{-\Delta}}{2}\overline{\tau} + c_2 \sin\frac{\sqrt{-\Delta}}{2}\overline{\tau}\right)e^{-\left(\zeta\Pi_\omega+\overline{\zeta}\Pi_{\omega 1}\right)\overline{\tau}} + \frac{\sqrt{-\Delta}}{2}\left(-c_1 \sin\frac{\sqrt{-\Delta}}{2}\overline{\tau} + c_2 \cos\frac{\sqrt{-\Delta}}{2}\overline{\tau}\right)e^{-\left(\zeta\Pi_\omega+\overline{\zeta}\Pi_{\omega 1}\right)\overline{\tau}} \quad (21)$$

where

$$\Delta = 4\left[\left(\zeta\Pi_\omega + \overline{\zeta}\Pi_{\omega 1}\right)^2 - \left(\Pi_\omega^2 + \Pi_{\omega 1}^2\right)\right] \quad \Delta < 0 \quad (22)$$

and c_1 and c_2 = unknown constants to be determined by the initial conditions

$$\overline{\tau} = 0, \quad \delta(0) = 0, \quad \dot{\delta}(0) = v_0 \quad (23)$$

where v_0 = dimensionless initial velocity of the oscillator when impact occurs. By substituting Eq. (23) into Eqs. (20) and (21), the constants c_1 and c_2 can be easily solved

$$c_1 = 0, \quad c_2 = \frac{2v_0}{\sqrt{-\Delta}} \quad (24)$$

Based on Eqs. (20) and (24), the normalized penetration displacement can be obtained as

$$\delta(\overline{\tau}) = e^{-\left(\zeta\Pi_\omega+\overline{\zeta}\Pi_{\omega 1}\right)\overline{\tau}}\frac{2v_0}{\sqrt{-\Delta}}\sin\frac{\sqrt{-\Delta}}{2}\overline{\tau} \quad (25)$$

From Eq. (25), if the penetration displacement returns at zero [i.e., $\sin(\sqrt{-\Delta}/2)\overline{\tau} = 0$], the result is $\overline{\tau} = 2n\pi/\sqrt{-\Delta}$; therefore, the first time the oscillator is separated from the barrier is $\overline{\tau} = 2\pi/\sqrt{-\Delta}$, which means that the time during contact is $\Delta\tau = 2\pi/\sqrt{-\Delta}$.

Solution for Oscillator's Pounding Response

When $x - \Pi_d \geq 0$, the oscillator contacts the barrier. According to Eqs. (12) and (17), the motion equation during the contact process can be written as

$$\ddot{x} + 2\left(\zeta\Pi_\omega + \overline{\zeta}\Pi_{\omega 1}\right)\dot{x} + \left(\Pi_\omega^2 + \Pi_{\omega 1}^2\right)x = -\sin\tau + \Pi_{\omega 1}^2\Pi_d \quad (26)$$

The initial conditions are set as the oscillator just makes contact with the barrier; therefore

$$\begin{aligned} &\tau = \tau_0, \quad x(\tau_0) = \Pi_d, \quad \dot{x}(\tau_0) = v_0 \\ &\tau = \tau_0 + \Delta\tau, \quad x(\tau_0 + \Delta\tau) = \Pi_d, \quad \dot{x}(\tau_0 + \Delta\tau) = -rv_0 \end{aligned} \quad (27)$$

where τ_0 = dimensionless time that the contact just occurs; and $\Delta\tau = 2\pi/\sqrt{-\Delta}$ = dimensionless time during contact.

The solutions for Eq. (26) are

$$\begin{aligned} x(\tau) &= e^{-\left(\zeta\Pi_\omega+\overline{\zeta}\Pi_{\omega 1}\right)(\tau-\tau_0)}\left[c_1' \cdot \cos\frac{\sqrt{-\Delta}}{2}(\tau-\tau_0) + c_2' \cdot \sin\frac{\sqrt{-\Delta}}{2}(\tau-\tau_0)\right] + A' \cdot \cos\tau + B' \cdot \sin\tau + \frac{\Pi_{\omega 1}^2 \cdot \Pi_d}{\Pi_\omega^2 + \Pi_{\omega 1}^2} \\ \dot{x}(\tau) &= e^{-\left(\zeta\Pi_\omega+\overline{\zeta}\Pi_{\omega 1}\right)(\tau-\tau_0)}\left(-\zeta\Pi_\omega - \overline{\zeta}\Pi_{\omega 1}\right)\left[c_1' \cdot \cos\frac{\sqrt{-\Delta}}{2}(\tau-\tau_0) + c_2' \cdot \sin\frac{\sqrt{-\Delta}}{2}(\tau-\tau_0)\right] \\ &\quad + e^{-\left(\zeta\Pi_\omega+\overline{\zeta}\Pi_{\overline{\omega}}\right)(\tau-\tau_0)}\left(\frac{\sqrt{-\Delta}}{2}\right)\left[-c_1' \cdot \sin\frac{\sqrt{-\Delta}}{2}(\tau-\tau_0) + c_2' \cdot \cos\frac{\sqrt{-\Delta}}{2}(\tau-\tau_0)\right] - A' \cdot \sin\tau + B' \cdot \cos\tau \end{aligned} \quad (28)$$

where

$$A' = \frac{2\left(\zeta\Pi_\omega + \overline{\zeta}\Pi_{\omega 1}\right)}{4\left(\zeta\Pi_\omega + \overline{\zeta}\Pi_{\omega 1}\right)^2 + \left(\Pi_\omega^2 + \Pi_{\omega 1}^2 - 1\right)^2} \quad \text{and}$$
$$B' = \frac{1 - \Pi_\omega^2 - \Pi_{\omega 1}^2}{4\left(\zeta\Pi_\omega + \overline{\zeta}\Pi_{\omega 1}\right)^2 + \left(\Pi_\omega^2 + \Pi_{\omega 1}^2 - 1\right)^2} \quad (29)$$

and the constants c_1' and c_2' can be obtained based on the initial conditions by substituting Eq. (28) into Eq. (27). In addition, $\sin(\sqrt{-\Delta}/2)\Delta\tau = \sin\pi = 0$, and $\cos(\sqrt{-\Delta}/2)\Delta\tau = \cos\pi = -1$. The four initial conditions in Eq. (27) can be written as

$$c_1' + A' \cdot \cos\tau_0 + B' \cdot \sin\tau_0 = \frac{\Pi_\omega^2 \cdot \Pi_d}{\Pi_\omega^2 + \Pi_{\omega 1}^2} \quad (30)$$

$$\left(-\zeta\Pi_\omega - \overline{\zeta}\Pi_{\omega 1}\right) \cdot c_1' + \left(\frac{\sqrt{-\Delta}}{2}\right) \cdot c_2' - A' \cdot \sin\tau_0 + B' \cdot \cos\tau_0 = v_0 \quad (31)$$

$$-c_1' e^{-\left(\zeta\Pi_\omega+\overline{\zeta}\Pi_{\omega 1}\right)\Delta\tau} + A' \cdot \cos(\tau_0 + \Delta\tau) + B' \cdot \sin(\tau_0 + \Delta\tau) = \frac{\Pi_\omega^2 \cdot \Pi_d}{\Pi_\omega^2 + \Pi_{\omega 1}^2} \quad (32)$$

$$e^{-\left(\zeta\Pi_\omega+\overline{\zeta}\Pi_{\omega 1}\right)\Delta\tau} \cdot \left(\zeta\Pi_\omega + \overline{\zeta}\Pi_{\overline{\omega}}\right) \cdot c_1' - e^{-\left(\zeta\Pi_\omega+\overline{\zeta}\Pi_{\omega 1}\right)\Delta\tau} \cdot \left(\frac{\sqrt{-\Delta}}{2}\right) \cdot c_2' - A' \cdot \sin(\tau_0 + \Delta\tau) + B' \cdot \cos(\tau_0 + \Delta\tau) = -rv_0 \quad (33)$$

Constant c_1' can be easily solved from Eq. (30) as

$$c_1' = \frac{\Pi_\omega^2 \cdot \Pi_d}{\Pi_\omega^2 + \Pi_{\omega 1}^2} - A' \cdot \cos\tau_0 - B' \cdot \sin\tau_0 \quad (34)$$

If v_0 is eliminated between Eqs. (31) and (33), then the constant c_2' can be obtained as

$$c_2' = \frac{2\left(\zeta\Pi_\omega + \bar{\zeta}\Pi_{\omega 1}\right)c_1'}{\sqrt{-\Delta}} + \frac{a_2}{\left(e^{-\left(\zeta\Pi_\omega+\bar{\zeta}\Pi_{\omega 1}\right)\Delta\tau} - r\right)\left(\sqrt{-\Delta}/2\right)} \tag{35}$$

where

$$a_2 = -A'\sin(\tau_0+\Delta\tau) + B'\cos(\tau_0+\Delta\tau) - rA'\sin\tau_0 + rB'\cos\tau_0 \tag{36}$$

The objective then is to solve for τ_0. By substituting Eq. (34) into Eq. (32) and then eliminating c_1', an expression for τ_0 is obtained

$$w_1\cdot\sin\tau_0 + w_2\cdot\cos\tau_0 = w_3 \tag{37}$$

where

$$w_1 = B'e^{-\left(\zeta\Pi_\omega+\bar{\zeta}\Pi_{\omega 1}\right)\Delta\tau} - A'\sin\Delta\tau + B'\cos\Delta\tau \tag{38}$$

$$w_2 = A'e^{-\left(\zeta\Pi_\omega+\bar{\zeta}\Pi_{\omega 1}\right)\Delta\tau} + A'\cos\Delta\tau + B'\sin\Delta\tau \tag{39}$$

$$w_3 = \left(e^{-\left(\zeta\Pi_\omega+\bar{\zeta}\Pi_{\omega 1}\right)\Delta\tau} + 1\right)\cdot\frac{\Pi_\omega^2\cdot\Pi_d}{\Pi_\omega^2+\Pi_{\omega 1}^2} \tag{40}$$

The solution to τ_0 in Eq. (37) is

$$\tau_0 = \sin^{-1}\left(\frac{w_3}{\sqrt{w_1^2+w_2^2}}\right) - \tan^{-1}\left(\frac{w_2}{w_1}\right) \tag{41}$$

This value of τ_0 then can be used in Eq. (31) to find v_0. Note that the multiple branches of both the $\sin^{-1}$ and $\tan^{-1}$ functions imply the existence of multiple solutions for τ_0. Only appropriate solutions for which τ_0 lies between 0 and $2n\pi$ and for which $v_0>0$ should be accepted. A positive v_0 guarantees that the oscillator collides with the barrier in the positive direction. The parameter n means that one impact occurs in every n cycles of excitation. To this end, the response of the oscillator in the contact phase is solved. In the next section, the response of the oscillator detached and away from the barrier is analyzed.

Solution for Oscillator's Response between Impacts

The equation for the motion of the oscillator in the noncontact phase can be derived by substituting Eq. (17) into Eq. (13)

$$\ddot{x} + 2\zeta\Pi_\omega\dot{x} + \Pi_\omega^2 x = -\sin\tau \tag{42}$$

The initial conditions are set as the state of the oscillator immediately after an impact

$$\tau = \tau_0+\Delta\tau,\quad x(\tau_0+\Delta\tau) = \Pi_d,\quad \dot{x}(\tau_0+\Delta\tau) = -rv_0 \tag{43}$$

where $\tau = \tau_0+\Delta\tau$ = dimensionless time when the oscillator is just detached from the barrier; and $-rv_0$ = dimensionless velocity of the oscillator at that moment. The velocity can be obtained by solving Eq. (33).

The solution to Eq. (42) can be expressed as

$$x(\tau) = e^{-\zeta\Pi_\omega(\tau-\tau_0)}\cdot\left[c_3\cdot\cos\sqrt{1-\zeta^2}\Pi_\omega(\tau-\tau_0) + c_4\cdot\sin\sqrt{1-\zeta^2}\Pi_\omega(\tau-\tau_0)\right] + A\cdot\cos\tau + B\cdot\sin\tau \tag{44}$$

$$\dot{x}(\tau) = e^{-\zeta\Pi_\omega(\tau-\tau_0)}\cdot(-\zeta\Pi_\omega)\cdot\left[c_3\cos\sqrt{1-\zeta^2}\Pi_\omega(\tau-\tau_0) + c_4\sin\sqrt{1-\zeta^2}\Pi_\omega(\tau-\tau_0)\right] + e^{-\zeta\Pi_\omega(\tau-\tau_0)}\cdot\left(\sqrt{1-\zeta^2}\Pi_\omega\right)\cdot\left[-c_3\sin\sqrt{1-\zeta^2}\Pi_\omega(\tau-\tau_0) + c_4\cos\sqrt{1-\zeta^2}\Pi_\omega(\tau-\tau_0)\right] + B\cdot\cos\tau - A\cdot\sin\tau \tag{45}$$

where

$$A = \frac{2\zeta\Pi_\omega}{(2\zeta\Pi_\omega)^2 + \left(\Pi_\omega^2-1\right)^2}\quad\text{and}\quad B = \frac{1-\Pi_\omega^2}{(2\zeta\Pi_\omega)^2 + \left(\Pi_\omega^2-1\right)^2} \tag{46}$$

Substituting $\tau = \tau_0+\Delta\tau$ into Eqs. (44) and (45) and then introducing in the results the initial conditions of Eq. (43) gives

$$e^{-\zeta\Pi_\omega\Delta\tau}\cdot\left(c_3\cdot\cos\sqrt{1-\zeta^2}\Pi_\omega\Delta\tau + c_4\cdot\sin\sqrt{1-\zeta^2}\Pi_\omega\Delta\tau\right) + A\cos(\tau_0+\Delta\tau) + B\sin(\tau_0+\Delta\tau) = \frac{d}{l_e} \tag{47}$$

$$e^{-\zeta\Pi_4\Delta\tau}\cdot(-\zeta\Pi_\omega)\cdot\left(c_3\cos\sqrt{1-\zeta^2}\Pi_\omega\Delta\tau + c_4\sin\sqrt{1-\zeta^2}\Pi_\omega\Delta\tau\right) + e^{-\zeta\Pi_\omega\Delta\tau}\cdot\left(\sqrt{1-\zeta^2}\Pi_\omega\right)\cdot\left(-c_3\sin\sqrt{1-\zeta^2}\Pi_\omega\Delta\tau + c_4\cos\sqrt{1-\zeta^2}\Pi_\omega\Delta\tau\right) + B\cos(\tau_0+\Delta\tau) - A\sin(\tau_0+\Delta\tau) = -rv_0 \tag{48}$$

From Eqs. (47) and (48), two unknown constants c_3 and c_4 can be obtained

$$c_3 = p_1\cdot\cos\sqrt{1-\zeta^2}\Pi_\omega\Delta\tau - p_2\cdot\sin\sqrt{1-\zeta^2}\Pi_\omega\Delta\tau \tag{49}$$

$$c_4 = p_1\cdot\sin\sqrt{1-\zeta^2}\Pi_\omega\Delta\tau + p_2\cdot\cos\sqrt{1-\zeta^2}\Pi_\omega\Delta\tau \tag{50}$$

where

$$p_1 = b_2'e^{\zeta\Pi_\omega\Delta\tau} \tag{51}$$

$$p_2 = \frac{\zeta\Pi_\omega b_2' + b_3'}{\sqrt{1-\zeta^2}\cdot\Pi_\omega}e^{\zeta\Pi_\omega\Delta\tau} \tag{52}$$

$$b_2' = \Pi_d - A\cos(\tau_0 + \Delta\tau) - B\sin(\tau_0 + \Delta\tau) \quad (53)$$

$$b_3' = \zeta\Pi_\omega b_2' + A\sin(\tau_0 + \Delta\tau) - B\cos(\tau_0 + \Delta\tau) - rv_0 \quad (54)$$

Hence, the analytical solutions for steady-state periodic impacts of the oscillator during the phases of contact and noncontact are solved. In addition, the analytical solution for the transient part of the pounding response is not considered in this work, which is also important in the case of seismic excitation. The transient part response for real recorded ground motions will be investigated by other methods (e.g., the numerical method) in future research work.

Verification of Analytical Solution

To verify our analytical solution for impact, the fourth-order Runge-Kutta method with an adaptive step size control is used to integrate Eq. (8) numerically, and a time step equal to 0.001 has been used (Press et al. 1992). Modal damping of 5% is assigned to the oscillator. Subsequently, the analytical solutions derived in the preceding section are compared with the steady-state numerical results. Davis (1992) proposed that after the numerical simulations for 40 cycles of excitation periods, the recorded impacts for a further eight cycles should be used as the steady-state response. This treatment is adopted herein for the verification that follows.

The numerically and analytically obtained dimensionless maximum displacement Π_u and velocity Π_v as functions of Π_ω are illustrated in Figs. 3(a and b), respectively. In addition, the dimensionless displacement and velocity spectra for a single oscillator without pounding are also included (*no-pounding*). Fig. 3 shows that the analytical solutions match well with the numerical results, especially in the region of $\Pi_\omega \geq 1$. When the dimensionless frequency is $0.4 < \Pi_\omega < 1$, some discrepancies can be observed. The reasons for the discrepancies are partly the result of the fact that the analytical solution is not applicable to the case of nonperiodic or chaotic impacts that may arise in this frequency region. Other possible reasons include the unavoidable truncation error as well as the round-off error. However, the discrepancies between the analytical and numerical solutions are acceptable and could demonstrate the accuracy of the analytical solution. The analytical solution yields a reasonable approximation to the numerically generated data.

The effect of pounding on Π_u is evident through comparison of the pounding case with the no-pounding case in Fig. 3(a). Three distinct spectral regions are identified empirically. The first region is $0 < \Pi_\omega < 0.75$, implying a relatively flexible structure colliding with the rigid barrier. Within this region, the pounding tends to amplify the maximum displacement of the oscillator. The second region is characterized by $0.75 \leq \Pi_\omega \leq 1.6$, wherein Π_u is obviously decreased as a result of pounding. Notably, structural resonance is hindered within this region because of the significant pounding-related energy absorption. The third region is $\Pi_\omega > 1.6$, implying a relatively rigid structure. In this case, the pounding has a negligible effect on the structural response. At a very large dimensionless frequency (e.g., $\Pi_\omega \geq 4$), the structure nearly vibrates as an inclusion of the ground, yielding almost no relative displacement Π_u and hence no pounding.

The maximum velocity response Π_v, shown in Fig. 3(b), has presented three similar distinct spectral regions as in the displacement spectrum. In the first region ($0 < \Pi_\omega < 0.75$), Π_v is amplified because of pounding. In the second region ($0.75 \leq \Pi_\omega \leq 1.3$), pounding diminishes the maximum velocity. In the third region ($\Pi_\omega > 1.3$), it is noticed that the velocity is slightly amplified as a result of pounding when $1.3 < \Pi_\omega < 3$, whereas the displacement appears nearly unaffected in this region. This can be attributed to the fact that the change in velocity is so small that it fails to alter the displacement in this region. When $\Pi_\omega \geq 3$, there is a negligible effect of pounding.

The significance of applying the dimensional analysis is presented in Fig. 4, where the oscillator is subjected to excitation at different intensity levels: $a_p = 0.2, 0.5,$ and $0.8g$. Fig. 4(a) plots the velocity spectra with real physical units; Fig. 4(b) gives the corresponding response in the dimensionless form. Note that the response velocity curves are reduced into a single master curve when plotted in terms of the dimensionless Π-terms. This observation indicates that the normalized response is invariant with respect to changes in the acceleration amplitude a_p. This scale invariance is known as self-similarity (Langhaar 1951; Barenblatt 1996). The concept of self-similarity is the main advantage of the dimensional analysis used in this paper. The usefulness of such reduction is also reflected by dealing with the parametric complexity in the research field of earthquake-induced pounding, through which application of the dimensional analysis method offers a lucid interpretation of the response of a pounding oscillator.

Parametric Analysis of Pounding

Effect of Contact Stiffness

In this study, the influence of contact stiffness on the pounding response is investigated by means of the frequency $\Pi_{\omega 1}$. Fig. 5 shows the normalized maximum penetration displacement Π_{ucon} versus the frequency ratio Π_ω for various $\Pi_{\omega 1}$ with respect to four different values of dimensionless gap Π_d. As shown in Fig. 5, the penetration displacement decreases notably with an increase in $\Pi_{\omega 1}$. Noticeably, large penetration displacement values can be unrealistically observed in the first spectral region when $\Pi_{\omega 1} < 50$. Thus, to avoid unrealistic penetration, small contact stiffness values should not be

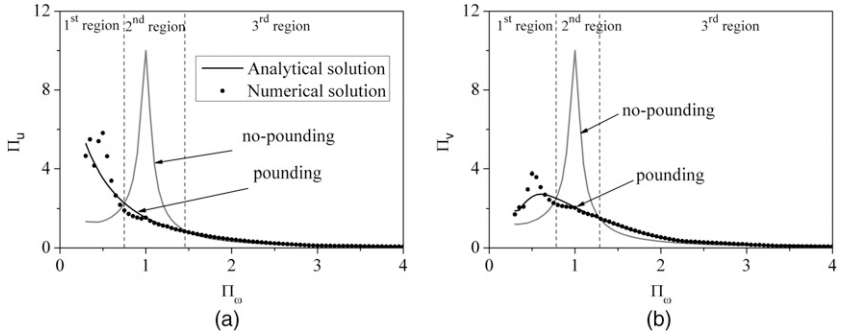

Fig. 3. Numerical and analytical dimensionless displacement and velocity spectra versus Π_ω for $\Pi_\zeta = 0.05$, $\Pi_r = 0.4$, $\Pi_{\omega 1} = 100$, and $\Pi_d = 0.1$

J. Eng. Mech., 2015, 141(4): 04014138

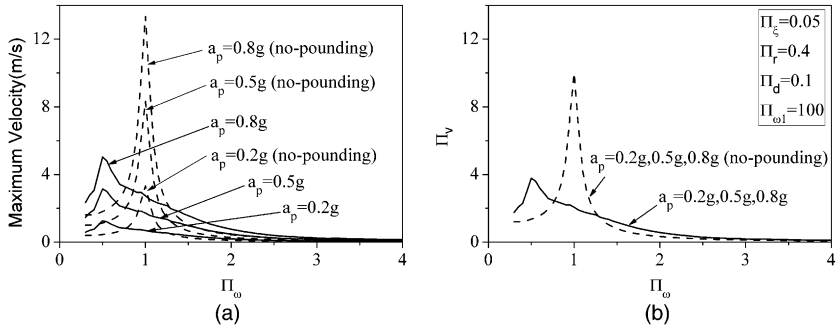

Fig. 4. (a) Dimensional maximum velocity response of pounding oscillator subject to different amplitudes of excitation; (b) dimensionless maximum velocity response by employing dimensionless Π-terms

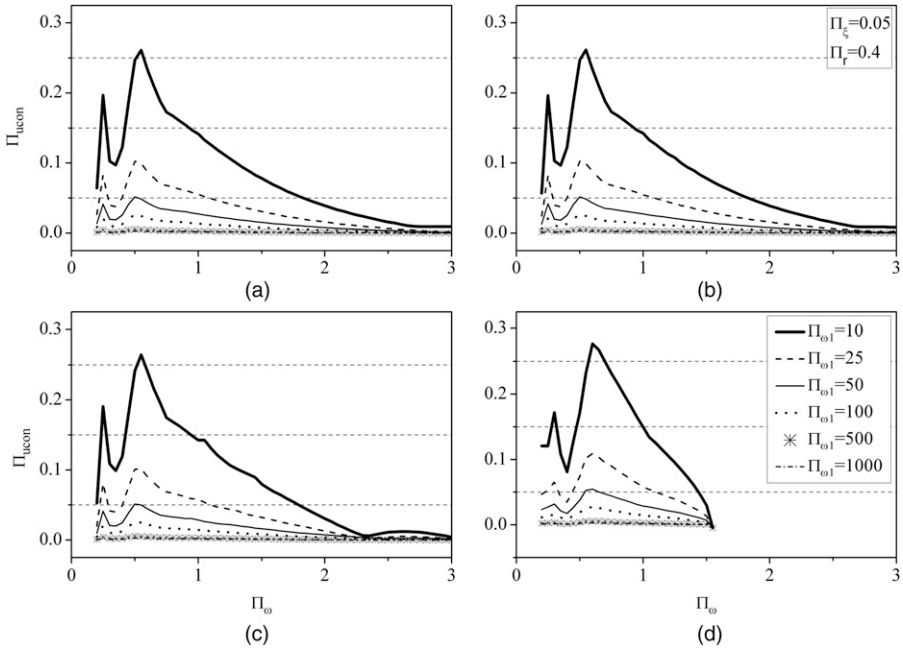

Fig. 5. Maximum penetration displacement spectra versus Π_ω for various frequency ratios $\Pi_{\omega 1}$ with respect to four different values of dimensionless gap Π_d: (a) $\Pi_d = 0.001$; (b) $\Pi_d = 0.01$; (c) $\Pi_d = 0.1$; (d) $\Pi_d = 1$

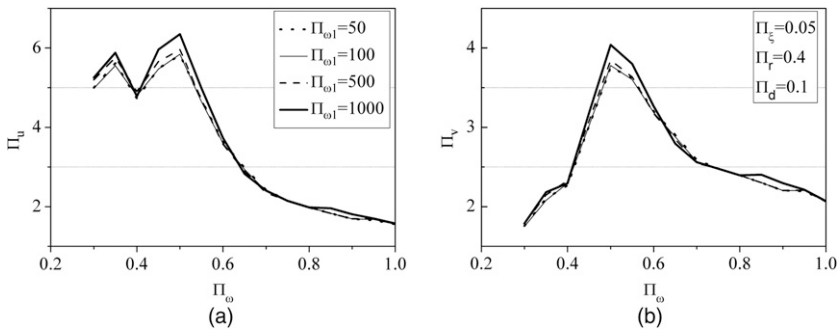

Fig. 6. Maximum dimensionless displacement Π_u and velocity Π_v versus Π_ω for various frequency ratios $\Pi_{\omega 1}$

used. What's more, it is indicated that penetration displacement tends to zero when the frequency ratio $\Pi_{\omega 1} \geq 500$, meaning that there is nearly no deformation if the contact stiffness is too large. As Π_d increases, the chance of pounding is reduced for a large frequency ratio Π_ω in the third spectral region. As Fig. 5(d) demonstrates, when Π_d reaches 1, no collision happens when $\Pi_\omega \geq 1.6$. In the first and second spectral regions, the effect of contact stiffness on the penetration displacement for different gap sizes is almost the same.

Figs. 6(a and b) show the dimensionless maximum displacement Π_u and the maximum velocity Π_v versus the frequency ratio Π_ω for

various $\Pi_{\omega 1}$, respectively. It is noted that the displacement Π_u and the velocity Π_v in the first spectral region are slightly affected by $\Pi_{\omega 1}$. In general, larger $\Pi_{\omega 1}$ leads to larger Π_u and Π_v. In addition, the effect of $\Pi_{\omega 1}$ on the pounding response is not apparent when $\Pi_{\omega 1} \geq 500$. In the second and third spectral regions, the displacement Π_u and velocity Π_v of the oscillator are almost invariable for all the values of $\Pi_{\omega 1}$, which is consistent with previous studies (Anagnostopoulos 1988; Maison and Kasai 1992), implying that the system response is insensitive to changes in contact stiffness. The displacement Π_u and velocity Π_v come to peak values when Π_ω approaches 0.5.

Effect of Coefficient of Restitution

The dimensionless coefficient of restitution is Π_r, and it has a unique significance in impact. The case of $\Pi_r = 1$ stands for a fully elastic collision, whereas the case of $\Pi_r = 0$ denotes a fully plastic collision. Pounding results in energy loss; thus, the coefficient of restitution Π_r should be less than 1. In fact, the value of $\Pi_r = 0.65$ has been used in a number of numerical analyses (Jankowski 2008; Anagnostopoulos 1988). On the other hand, the experimental study conducted by Zhu et al. (2002) shows that the value of Π_r can be as low as 0.4. In this paper, $\Pi_r = 0.001, 0.4, 0.65$, and 1 are chosen to study the effect of the coefficient of restitution on pounding response.

Fig. 7 plots the relationship between normalized maximum penetration displacement Π_{ucon} and the frequency ratio Π_ω for various $\Pi_{\omega 1}$ and different values of Π_r. It can be seen that when $\Pi_{\omega 1} < 500$, the effect of contact stiffness on the penetration displacement is obviously influenced by the change in Π_r. As Π_r increases, the penetration displacement increases. It is observed that the maximum penetration displacement for $\Pi_r = 0.001$ is obviously much smaller than the Π_{ucon} caused by greater Π_r in the first and second spectral regions. This may be explained by the fact that the response for $\Pi_r = 0.001$ is close to a fully plastic collision, and the corresponding penetration displacement decreases rapidly because of great energy dissipation. For $\Pi_r = 0.4$ and 0.65, unrealistically large penetration displacement values can be observed when $\Pi_{\omega 1} < 100$. As Π_r grows up to 1, there is no energy dissipation during the collision, and much larger Π_{ucon} can be seen when $\Pi_{\omega 1} < 500$. In addition, when $\Pi_{\omega 1} \geq 500$, the penetration displacement is nearly unaffected by Π_r.

Figs. 8(a and b) show the normalized maximum displacement Π_u and maximum velocity Π_v spectra versus Π_ω for different values of

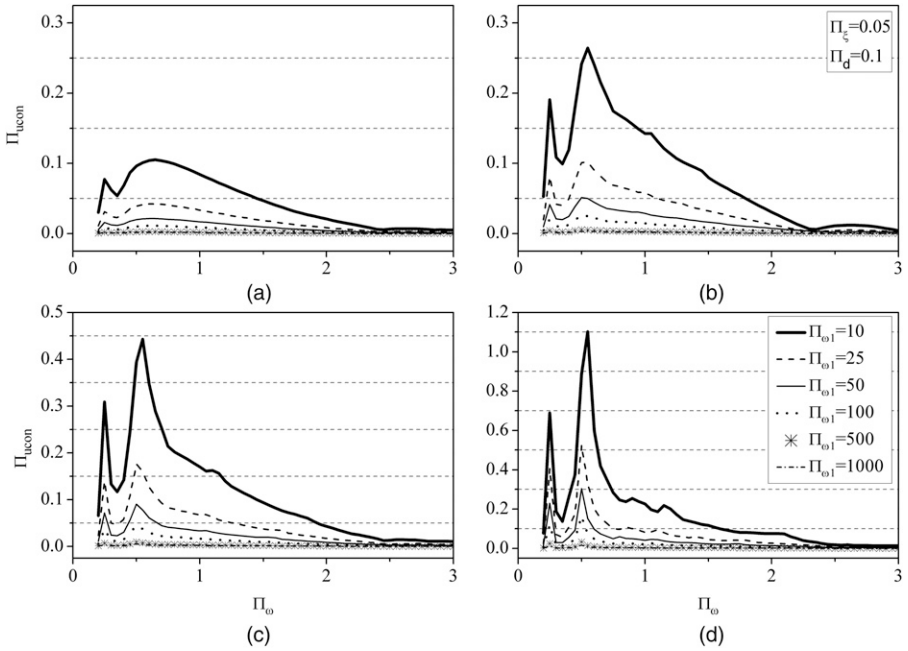

Fig. 7. Maximum penetration displacement spectra versus Π_ω for various frequency ratios $\Pi_{\omega 1}$ with respect to four different values of dimensionless coefficient of restitution Π_r: (a) $\Pi_r = 0.001$; (b) $\Pi_r = 0.4$; (c) $\Pi_r = 0.65$; (d) $\Pi_r = 1$

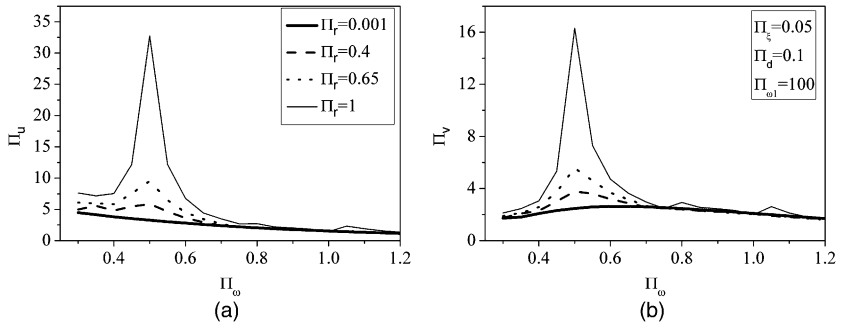

Fig. 8. Maximum dimensionless displacement Π_u and velocity Π_v spectra versus Π_ω for various Π_r

Π_r, respectively. It is seen that the displacement and velocity increase significantly for larger Π_r in the first spectral region, whereas the responses in other spectral regions are almost identical irrespective of the variation in Π_r. The results shown in Fig. 8 are similar to the conclusion in the literature (Ruangrassamee and Kawashima 2001) that neglecting energy dissipation resulting from impact ($\Pi_r = 1$) overestimates the responses of the colliding system. The counterintuitive behavior observed in the work of Dimitrakopoulos et al. (2009) is not found in this work, and this may be attributed to the difference in the excitation input and method of simulating the contact. The displacement Π_u and velocity Π_v come to peak values when Π_ω tends to 0.5.

Conclusions

In this paper, the dynamic response of a single pounding oscillator subjected to harmonic excitations is investigated with dimensional analysis with an explicit consideration of the contact process. A linear viscoelastic impact model is used to simulate the pounding force. Dimensional analysis leads to a condensed presentation of the response and parametric analysis. The introduction of Buckingham's Π theorem reduces the number of variables governing the response from eight to six. When the response is presented in terms of the dimensionless Π-terms, the response curves are self-similar and follow a single master curve. This unveils the remarkable property of self-similarity—a special type of symmetry that is invariant with respect to changes in scale or size. Analytical solutions for dimensionless contact time, impact displacement, and velocity expressed by the dimensionless Π-terms are derived in this study and agree qualitatively with the numerical simulations.

The effect of contact stiffness is studied through the frequency ratio $\Pi_{\omega 1}$. The peak value of displacement and the velocity are nearly unaffected by the contact stiffness. The penetration displacements for different levels of contact stiffness ($\Pi_{\omega 1}$ values) are insensitive to the dimensionless gap size Π_d but are affected significantly by the changes in the coefficient of restitution Π_r.

In this study, to arrive at a conclusion in a convenient and feasible way, the pounding response for harmonic excitation is considered. To obtain a more realistic dimensionless pounding response under earthquake excitation, the pounding responses for real recorded ground motions need further investigation in future research.

Acknowledgments

The authors express their sincere gratitude to Shuang Li, Zhiwang Chang, and Lili Xie of the Harbin Institute of Technology for their help. This research was supported by the Program for International Science and Technology Cooperation Projects of China (Grant No. 2012DFA70810), the National Natural Science Foundation of China (Grant Nos. 51238012, 91215301, and 51008101), and the Program for New Century Excellent Talents in University of the Ministry of Education of China (Grant No. NCET-11-0813).

References

Anagnostopoulos, S. A. (1988). "Pounding of buildings in series during earthquakes." *Earthquake Eng. Struct. Dyn.*, 16(3), 443–456.

Anagnostopoulos, S. A. (1995). "Earthquake induced pounding: State of the art." *Proc., 10th European Conf. on Earthquake Engineering*, G. Duma, ed., Vol. 2, Balkema, Rotterdam, Netherlands, 897–905.

Anagnostopoulos, S. A. (1996). "Building pounding re-examined: How serious a problem is it?" *Proc., 11th World Conf. on Earthquake Engineering* (CD-ROM), Elsevier Science, Amsterdam, Netherlands.

Anagnostopoulos, S. A. (2004). "Equivalent viscous damping for modeling inelastic impacts in earthquake pounding problems." *Earthquake Eng. Struct. Dyn.*, 33(8), 897–902.

Anagnostopoulos, S. A., and Spiliopoulos, K. V. (1992). "An investigation of earthquake induced pounding between adjacent buildings." *Earthquake Eng. Struct. Dyn.*, 21(4), 289–302.

Athanassiadou, C. J., Penelis, G. G., and Kappos, A. J. (1994). "Seismic response of adjacent buildings with similar or different dynamic characteristics." *Earthquake Spectra*, 10(2), 293–317.

Barenblatt, G. I. (1996). *Scaling, self-similarity, and intermediate asymptotics*, Cambridge University Press, Cambridge, U.K.

Chau, K. T., and Wei, X. X. (2001). "Pounding of structures modeled as non-linear impacts of two oscillators." *Earthquake Eng. Struct. Dyn.*, 30(5), 633–651.

Comartin, C. D., Greene, M., and Tubbesing, S. K. (1995). "The Hyogo-ken Nanbu (Kobe) earthquake, January 17, 1995." *Preliminary Reconnaissance Rep. EERI-95-04*, Earthquake Engineering Research Institute, Oakland, CA.

Davis, R. O. (1992). "Pounding of buildings modelled by an impact oscillator." *Earthquake Eng. Struct. Dyn.*, 21(3), 253–274.

DesRoches, R., and Muthukumar, S. (2002). "Effect of pounding and restrainers on seismic response of multiple-frame bridges." *J. Struct. Eng.*, 10.1061/(ASCE)0733-9445(2002)128:7(860), 860–869.

Dimitrakopoulos, E., Makris, N., and Kappos, A. J. (2009). "Dimensional analysis of the earthquake-induced pounding between adjacent structures." *Earthquake Eng. Struct. Dyn.*, 38(7), 867–886.

Dimitrakopoulos, E., Makris, N., and Kappos, A. J. (2010). "Dimensional analysis of the earthquake response of a pounding oscillator." *J. Eng. Mech.*, 10.1061/(ASCE)0733-9399(2010)136:3(299), 299–310.

Dimitrakopoulos, E., Makris, N., and Kappos, A. J. (2011). "Dimensional analysis of the earthquake-induced pounding between inelastic structures." *Bull. Earthquake Eng.*, 9(2), 561–579.

Goldsmith, W. (1960). *Impact: The theory and physical behavior of colliding solids*, Edward Arnold, London.

Jankowski, R. (2005). "Non-linear viscoelastic modelling of earthquake-induced structural pounding." *Earthquake Eng. Struct. Dyn.*, 34(6), 595–611.

Jankowski, R. (2008). "Earthquake-induced pounding between equal height buildings with substantially different dynamic properties." *Eng. Struct.*, 30(10), 2818–2829.

Jankowski, R., Wilde, K., and Fujino, Y. (1998). "Pounding of superstructure segments in isolated elevated bridge during earthquakes." *Earthquake Eng. Struct. Dyn.*, 27(5), 487–502.

Jeng, V., and Tzeng, W. L. (2000). "Assessment of seismic pounding hazard for Taipei City." *Eng. Struct.*, 22(5), 459–471.

Kasai, K., and Maison, B. F. (1997). "Building pounding damage during the 1989 Loma Prieta earthquake." *Eng. Struct.*, 19(3), 195–207.

Langhaar, H. L. (1951). *Dimensional analysis and theory of models*, Wiley, New York.

Li, J. Z., Lu, X. L., Li, X., Ren, X., Liu, W., and Tang, Y. (2008). "Seismic damage of reinforced concrete frame structures in Wenchuan earthquake." *Struct. Eng.*, 24(3), 9–11.

Maison, B. F., and Kasai, K. (1992). "Dynamics of pounding when two buildings collide." *Earthquake Eng. Struct. Dyn.*, 21(9), 771–786.

Makris, N., and Black, C. J. (2004a). "Dimensional analysis of bilinear oscillators under pulse-type excitations." *J. Eng. Mech.*, 10.1061/(ASCE)0733-9399(2004)130:9(1019), 1019–1031.

Makris, N., and Black, C. J. (2004b). "Dimensional analysis of rigid-plastic and elastoplastic structures under pulse-type excitations." *J. Eng. Mech.*, 10.1061/(ASCE)0733-9399(2004)130:9(1006), 1006–1018.

Makris, N., and Psychogios, C. (2006). "Dimensional response analysis of yielding structures with first-mode dominated response." *Earthquake Eng. Struct. Dyn.*, 35(10), 1203–1224.

Malhotra, P. K. (1998). "Dynamics of seismic pounding at expansion joints of concrete bridges." *J. Eng. Mech.*, 10.1061/(ASCE)0733-9399(1998)124:7(794), 794–802.

Muthukumar, S., and DesRoches, R. (2006). "A Hertz contact model with non-linear damping for pounding simulation." *Earthquake Eng. Struct. Dyn.*, 35(7), 811–828.

Papadrakakis, M., Mouzakis, H., Plevris, N., and Bitzarakis, S. (1991). "A lagrange multiplier solution method for pounding of buildings during earthquakes." *Earthquake Eng. Struct. Dyn*, 20(11), 981–998.

Press, W. H., Flannery, B. P., Teukolsky, S. A., and Vetterling, W. T. (1992). *Numerical recipes: The art of scientific computing*, Cambridge University Press, New York.

Rosenblueth, E., and Meli, R. (1986). "The 1985 earthquake: Causes and effects in Mexico City." *Concr. Int.*, 8(5), 23–34.

Ruangrassamee, A., and Kawashima, K. (2001). "Relative displacement response spectra with pounding effect." *Earthquake Eng. Struct. Dyn.*, 30(10), 1511–1538.

Zhang, J., and Tang, Y. (2009). "Dimensional analysis of structures with translating and rocking foundations under near-fault ground motions." *Soil. Dyn. Earthquake Eng.*, 29(10), 1330–1346.

Zhu, P., Abe, M., and Fujino, Y. (2002). "Modelling three-dimensional non-linear seismic performance of elevated bridges with emphasis on pounding of girders." *Earthquake Eng. Struct. Dyn.*, 31(11), 1891–1913.